Journal of Engineering Mathematics **40:** 249–267, 2001.

A model for thermal Marangoni drying

O. ZIKANOV[1,*], W. BOOS[1], K. WOLKE[2] and A. THESS[3]
[1]*Institute for Aerospace Engineering, Department of Mechanical Engineering, Dresden University of Technology, 01062 Dresden, Germany*
[2]*STEAG MicroTech GmbH, 72124, Pliezhausen, Germany*
[3]*Department of Mechanical Engineering, Ilmenau University of Technology, P.O. Box 100565, 98684 Ilmenau, Germany*

Received 26 May 1999; accepted in revised form 10 August 2000

Abstract. The process of thermal Marangoni drying is considered, which has been recently proposed for use in semiconductor production. The process allows ultraclean drying of semiconductor wafer surfaces at the end of a sequence of wet operations. A theoretical model is presented, which incorporates the movement of a thin liquid film on the semiconductor surface, heat exchange between the semiconductor and outer medium, and the water flow below the meniscus. In the frame of this model, the problem is solved using a combination of lubrication approximation, one-dimensional heat transfer analysis, and spectral-element solution of the two-dimensional Stokes equations. Several examples are given to show how the model can be used to evaluate the efficiency of drying.

Key words: drying, Marangoni effect, lubrication theory, Stokes approximation

1. Introduction

The final stage of semiconductor processing includes a sequence of wet processes, the last one being rinsing in deionized water. After that, the semiconductor plate, called hereafter the wafer, has to be removed from the water in such a way that no water patches remain on the surface. This is extremely important because the patches can leave behind spots of pollution after the water evaporates. For the gravitational force alone to be able to fully strip the remaining film of water from the wafer surface, the withdrawal velocity of wafer must be very small, which reduces considerably the total production rate.

A novel technique for the rapid drying of the semiconductor surface that is becoming increasingly widespread (see *e.g.* [1–3]) during the last few years is Marangoni drying. This technique employs the Marangoni effect due to the variation of the surface-tension coefficient σ in the vicinity of the meniscus to increase the withdrawal velocity of wafers. In this particular case, a vertical gradient of σ leads to an additional stripping force acting on the remaining film of water. The experimental and theoretical studies [1–3] as well as experience of industrial application have shown that a sufficient surface-tension gradient can be achieved when a water soluble organic vapor (usually isopropyl alcohol – IPA) is added to the atmosphere. Drying devices based on this effect are successfully replacing the conventional techniques such as spin drying and vapor drying with boiling IPA.

*Present address: Department of Ocean Engineering, Florida Atlantic University, Boca Raton, FL 33431-0991.

The mechanism of Marangoni drying with IPA is relatively well understood (see *e.g.* [1], [3]). IPA acts like a surfactant. When adsorbed into water it lowers the surface tension. The dependence can be approximated by a linear relationship, namely

$$\sigma = \sigma_0 - \gamma_c c, \tag{1}$$

where c is the surfactant concentration at the surface and $\gamma_c > 0$ is a coefficient of surface-tension variation. Thus, the principal part of the Marangoni-drying technique is the creation of a vertical gradient of the surfactant concentration c. As discussed in detail in [3], this gradient is readily established at the water surface near the contact point between the entrained film and the meniscus. The surfactant diffuses quickly into the thin entrainment film above the contact point, whereas the diffusion below this point is lowered as the water layer becomes thicker.

As we already mentioned, Marangoni drying based on surface-tension variation due to variation in surfactant concentration is an established technique which is becoming increasingly widespread. In the present paper we address another type of Marangoni drying based on the dependence of surface tension on temperature (see [4]). Similar to (1) we can approximate the dependence by a linear function

$$\sigma = \sigma_0 - \gamma(T - T_0), \tag{2}$$

where T is the temperature at the surface and σ_0 is the surface tension corresponding to the reference temperature T_0. Obviously, the main goal of the drying technique now becomes the creation of a strong vertical temperature gradient at the surface of the entrained film.

We analyze a typical device for thermal Marangoni drying. The main goal is to create a simplified theoretical model, which can serve as a tool for a multi-parametric feasibility study of the process. The model has to provide an estimate of the asymptotic thickness h_0 of the water film as a function of macroscopic parameters of the system. Furthermore, the model has to be simple enough to make possible its repeated use for hundreds of combinations of these parameters. It has to be stressed that a direct numerical simulation of the whole system is impossible because of the extreme difference of typical length scales, such as the thickness of the remaining film $h_0 \sim 2$ μm and the gap width $D_0 \sim 2$ mm. These reasons dictate our approach to modeling as discussed in Section 2.

Our paper is the first to give a complete theoretical description of the process of thermal Marangoni drying. We consider all the important physical processes in the system dividing them into three groups in such a way that each group can be analysed separately using the most suitable modeling technique. It has to be stressed that the coupling between different processes is retained in the model in the reduced form of a combination of several input–output parameters.

The system under consideration and the model are described in Section 2. Some results are shown in Section 3 and the conclusions are given in Section 4.

2. System under consideration and theoretical model

2.1. System under consideration

We consider a system that, apart from the simplifications discussed below, corresponds to the typical Marangoni-drying facility used in semiconductor processing. A set of equally spaced, vertically positioned plates of a semiconducting material (wafers) is slowly withdrawn from

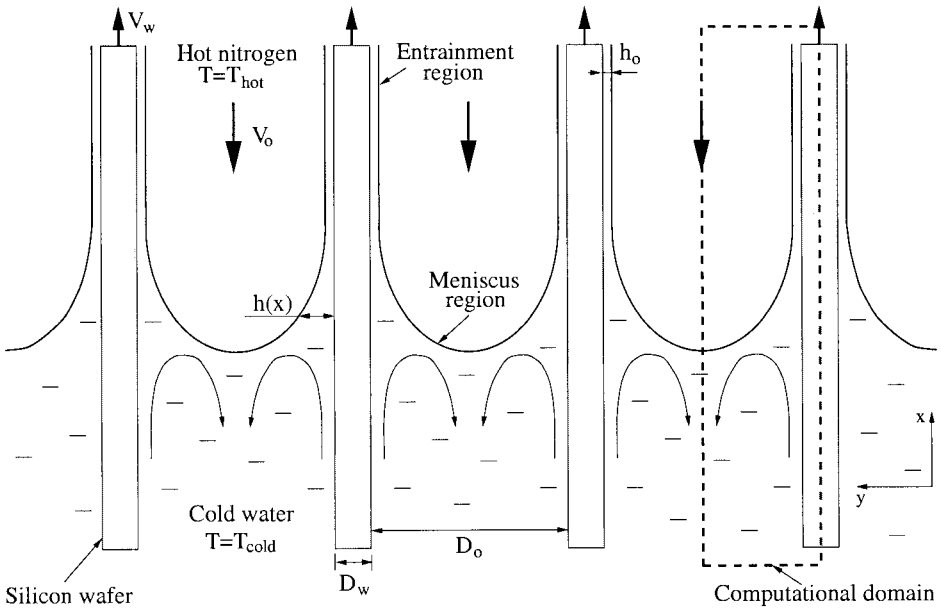

Figure 1. Marangoni drying facility: sketch of the two-dimensional model.

a tank of deionized water (see Figure 1). The typical wafer is usually a disk of thickness $D_w = 1$ mm and diameter 200 mm. The withdrawal velocity V_w varies from 1 mm s^{-1} to 4 mm s^{-1}. The distance between the wafers, which is determined by the design of the carrier, is usually $D_o = 3$mm.

The drying facility considered here was initially designed for the surfactant-based Marangoni-drying process. The working space above the water was closed by a transparent lid and filled with a mixture of nitrogen and isopropyl alcohol (IPA). Apart from facilitating the Marangoni effect, such an ultradry atmosphere provided for intensive water evaporation at the surface of the entrainment film. The permanent flow of the gas mixture was maintained while it was being pumped through the holes in the lid and allowed it to run out through the openings located in lateral walls near the water surface.

The same facility is used for thermal Marangoni drying considered in the present paper. The only difference is that the gas pumped under the lid is now pure ultradry nitrogen. There are many ways to create the necessary vertical temperature gradient required for maintaining the Marangoni force. In this paper, we consider two of them, both exploiting high thermal conductivity of the semiconductor and low (room) temperature of water in the tank:

(i) Gas Heating – nitrogen is preheated to high temperature and then pumped at a high flow rate into the working space. This results in a considerable temperature difference between the upper end of the wafer, which is heated due to the contact with nitrogen, and its lower end, which is cooled by water.

(ii) Contact Heating – instead of employing heat exchange with hot nitrogen one can heat the upper end of wafer directly with the help of a contact heater.

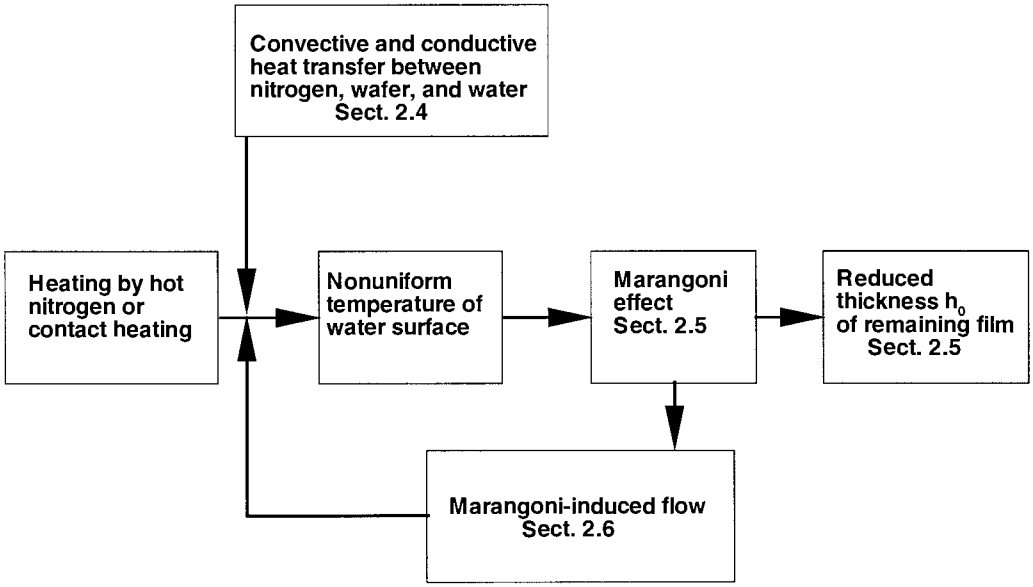

Figure 2. Principal physical mechanism of thermal Marangoni drying.

2.2. PHYSICAL MECHANISM OF THERMAL MARANGONI DRYING

The principal scheme of the complex physical mechanism of thermal Marangoni drying is given in Figure 2. The top part of the wafer is heated through heat exchange with the hot nitrogen pumped into the working space or through contact heating, while its bottom part is maintained at a much lower temperature due to contact with abundantly supplied cold water. The resulting vertical gradient of wafer temperature is a key phenomenon for the process of drying. It causes a nonuniform temperature distribution at the surface of the water drawn by the wafer and, thus, the Marangoni force. If the surface-temperature gradient is large enough, the 'stripping' action of the Marangoni force in the entrainment region can lead to considerable reduction of the asymptotic thickness h_0 of the remaining film.

For the drying process to be successful, h_0 has to be brought down to a threshold value, at which the evaporation and molecular forces are able to complete the 'patch-less' drying. The evaluation of this threshold is beyond the scope of this paper. Its value depends on the temperature and humidity of the atmosphere outside the film.

One can see in Figure 2 that the physical mechanism of thermal Marangoni drying is not limited to a straightforward scheme as outlined above. Essential complexity is added by intensive convective and conductive heat transfer between nitrogen, wafer, and water, all of them having different temperature distributions.

Another phenomenon to be considered is the water flow below the meniscus. The flow is driven by the Marangoni force at the surface and by the withdrawal motion of the wafer. The impact of the flow on the drying process is twofold. First, it introduces horizontal convective heat transfer, and, thus, causes redistribution of the surface temperature. Second, the flow pattern should furnish immediate removal of the particles washed off at the wafer wall. Therefore, development of any recirculation or stagnation zones near the wall is highly undesirable.

It has to be noted that one phenomenon, essential for the heat redistribution in the system, remains unaccounted for in our model. This is the flow of nitrogen in the gap between the

wafers. As a justification, we note that the flow has a complex even if, probably, laminar structure and, therefore, is difficult to simulate. On the other hand, the flow is predominantly in the vertical direction, and its particular pattern has only a limited influence on the heat exchange between the wafer and nitrogen.

2.3. Modeling approach

The sketch of the problem as it appears in our model is given in Figure 1. An important simplification is made – we neglect the dependence on a horizontal coordinate parallel to the wafer surface and solve a two-dimensional problem. Another simplification is based on the fact that the time scales of the physical processes governing the system behavior such as the horizontal thermal diffusion time D_o^2/κ or the time scale D_o/V based on the typical water velocity under the meniscus are much smaller than the typical time scale of the slow motion of the wafers. For this reason and because of the small Reynolds number (see below in this section), we adopt the quasi-static approximation and neglect the time-dependence of the solution.

Because of symmetry considerations, only the part of the system between the symmetry axes of a wafer and an adjacent gap is considered below. The x-axis is in the vertical direction, and the y-axis is directed horizontally, normal to the wafer surface. The surface $y = 0$ corresponds to the wafer wall. The origin of the x-axis is at the level of the lowest point of the meniscus except for the solution in the entrainment and transition regions in Section 2.5 where the origin is set to an imaginary contact point between these regions and the meniscus. Important parameters are the wafer width D_w, the gap between wafers D_o, and the wafer-withdrawal velocity V_w.

The model relies essentially on several simplifying assumptions, each of them valid with a very good degree of approximation in the case of the Marangoni-drying facility considered in this paper.

First, very small values of the capillary number are typical for the system, *i.e.*

$$\mathrm{Ca} \equiv \frac{V\mu}{\sigma_0} \ll 1. \tag{3}$$

In (3), μ is the dynamic viscosity and σ_0 is a mean value of the surface-tension coefficient (corresponding to a mean value of the surface temperature). For a typical velocity $V = V_w = 1$ mm s^{-1} we have $\mathrm{Ca} \approx 1{\cdot}2\times10^{-5}$.

Second, the typical thickness h_0 of the rest film is small in comparison with the thickness of the gap between the wafers and the typical length scale in the meniscus area, which is the capillary length

$$\ell_0 \equiv \left(\frac{2\sigma_0}{g\rho}\right)^{1/2}, \tag{4}$$

where g and ρ are, respectively, gravitational acceleration and water density.

Such a separation between the 'macroscale' ℓ_0 and 'microscale' h_0, as well as the smallness of the capillary number, allows us to use the method of matched asymptotic expansions when calculating the shape of the water free surface.

One more scale separation is between the typical horizontal and vertical scales of the flow. The small aspect ratio of the problem (width/height $\sim$ 0·15) leads to the possibility of neglecting the horizontal temperature variations in the wafer and the gap and obtaining

vertical distributions of horizontally averaged temperature by use of a the one-dimensional thermal analysis.

Next, an essential assumption is that both the macroscale and microscale Reynolds numbers are small,

$$\mathrm{Re}_{\ell_0} \equiv \frac{V\ell_0}{\nu} \ll 1, \qquad \mathrm{Re}_{h_0} \equiv \frac{Vh_0}{\nu} \ll 1, \tag{5}$$

where $\nu = \mu/\rho$ is the kinematic viscosity of water.

For $V = 1$mm/s, and $h_0 = 2\mu$m we have $\mathrm{Re}_{\ell_0} \approx 0{\cdot}3$ and $\mathrm{Re}_{h_0} \approx 2 \times 10^{-3}$. Therefore, the water flow can be approximately described by the Stokes equations

$$\nabla p = \mu \nabla^2 \boldsymbol{U} + \rho \boldsymbol{g}, \tag{6}$$

$$\nabla \cdot \boldsymbol{U} = 0. \tag{7}$$

The convection-diffusion equation for the temperature field $T(x, y)$ can be given as

$$\boldsymbol{U} \nabla T = \kappa \Delta T, \tag{8}$$

where κ is the thermal diffusivity of water.

The velocity boundary condition at the wafer wall $y = 0$ is (*cf.* Figure 1)

$$\boldsymbol{U} = V_w \boldsymbol{e}_x \quad \text{at} \quad y = 0, \tag{9}$$

and the conditions at the free surface $y = h(x)$ are

$$\boldsymbol{n} \cdot \hat{S} \cdot \boldsymbol{n} = \sigma\, K, \qquad \boldsymbol{\tau} \cdot \hat{S} \cdot \boldsymbol{n} = -\frac{\mathrm{d}\sigma}{\mathrm{d}s} = \gamma \frac{\mathrm{d}T}{\mathrm{d}s}, \qquad \boldsymbol{n} \cdot \boldsymbol{u} = 0, \quad \text{at } y = h(x), \tag{10}$$

where $\hat{S}$ is the total stress tensor, $\mathrm{d}/\mathrm{d}s$ stands for the gradient along the surface, and $\boldsymbol{n}$, $\boldsymbol{\tau}$, and K are, respectively, the normal and tangential unit vectors to the free surface and its curvature. The conditions (10) express the continuity of total stress and the stationarity of the free surface. The boundary conditions for the temperature field are discussed in Section 2.6 .

Based on the assumptions listed above, we divide the solution into three parts, each allowing a specific simplifying approach. They are the solution for the shape of the water free surface and the thickness of the entrained film, analysis of thermal fluxes between the water, wafer, and nitrogen, and simulation of the water flow and temperature distribution under the meniscus. It has to be stressed that these processes can not be completely separated. They are coupled with one another in a complex way through the temperature and velocity boundary conditions. In our model, the coupling is reduced to several most important parameters. This allows us to avoid the solution of the full problem involving widely separated length scales and achieve the best possible approximation for each process.

The vertical temperature distributions are determined in Section 2.4 through the one-dimensional thermal analysis.

The shape of free surface is evaluated in Section 2.5 using the lubrication approximation in the entrainment region and static solution for the meniscus. The small value of the macroscopic Reynolds number implies that we can neglect the influence of the water flow on the shape of the free surface. Another simplification is that, in Section 2.5, the temperature at the surface is considered constant everywhere, except in the thin entrainment region adjacent to the wafer.

The numerical simulation of the water flow based on the Equations (6–8) is presented in Section 2.6. By contrast to Section 2.5 we should take into account the temperature variance along the meniscus, since it creates the Marangoni force. This can have a great impact on the flow structure.

The coupling between the three separate parts of our analysis is as follows. The vertical temperature distributions in the wafer and the gap $T_w(x)$, $T_o(x)$, as provided by the one-dimensional thermal analysis, are used for defining the values of μ, σ_0, and $d\sigma/dx$ at the water surface. In a given geometry, these values completely determine the shape of the surface and the asymptotic thickness of the film h_0. Another use of $T_w(x)$, $T_o(x)$ is that they give the temperature boundary conditions for the water flow.

The free surface calculated in the framework of hydrostatic approximation is used as a boundary of the water-flow domain.

It can be shown by a simple scaling analysis and has been confirmed by our simulations that the influence of water flow on the vertical temperature distributions can be neglected. This allows us to avoid an iterative procedure and perform the study of a given configuration in the sequence:

(i) one-dimensional thermal analysis,
(ii) solution for the shape of free surface and entrained film,
(iii) simulation of the water flow.

We use everywhere the system of measurement units consisting of mm, g, s, and K for length, mass, time, and temperature, respectively. An exception is the discussion in Section 2.5 which is based on a scaling analysis and, thus, requires a non-dimensional presentation.

2.4. One-dimensional thermal analysis

In this section we derive a simple model which describes the processes of heat transfer between the wafer, water, and nitrogen and allows us to evaluate temperature distributions in these media. The model is based on the approach routinely used in engineering to analyze the processes of heat transfer in multi-layer systems. For our purpose, information on distributions in the vertical direction is of primary importance. Therefore, we make use of the small aspect ratio typical for the problem and formulate a one-dimensional model for the heat exchange processes in the water-wafer-nitrogen system.

We consider an idealized one-dimensional two-layer system consisting of a wafer and outer medium extending in a vertical direction between the points $x_b < 0$ (bottom) and $x_t > 0$ (top). An illustration is presented in Figure 3. The values of x_b and x_t can vary but their difference remains equal to the size of the wafer (200 mm in our calculations), and the point $x = 0$ always corresponds to the boundary between water and nitrogen. All the variables are averaged in the horizontal direction so that only the x-dependence is retained. $T_w(x)$ and $T_o(x)$ denote, respectively, the wafer temperature and the temperature of the outer medium. In a similar manner, we use the subscripts w and o to distinguish between the material constants of the wafer and the outer medium. Thermal conductivity, thermal diffusivity, density, and specific heat at constant pressure are denoted, respectively, by λ, $\kappa = \lambda/\rho c_p$, ρ, and c_p.

Another important parameter used in the model is V_o, the horizontally averaged vertical velocity of outer medium. The velocity of water can be taken equal to the wafer velocity V_w or set to zero. In either case, its value is typically very small and its influence on global heat exchange considered in this section is negligible. On the other hand, the velocity of nitrogen is very important, especially to the gas heating. We assume hereafter that the mean convective

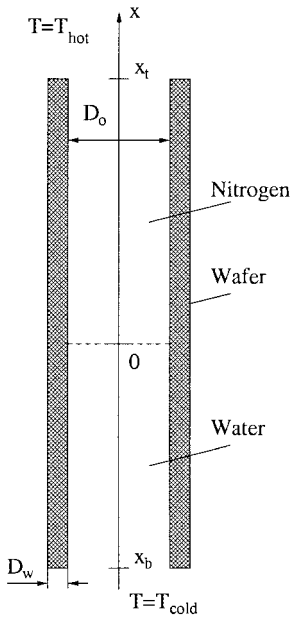

Figure 3. One-dimensional model for the heat exchange in the system water-wafer-nitrogen.

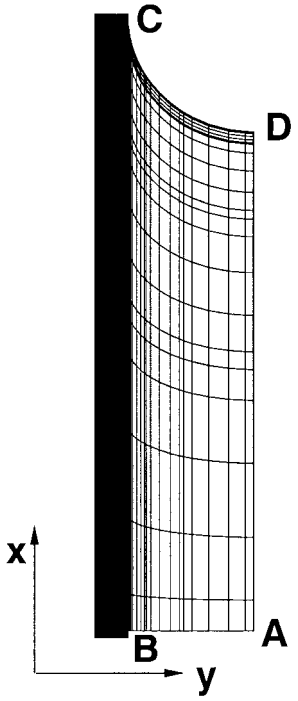

Figure 4. Computational domain and grid for the calculations of the meniscus flow.

heat transport in the vertical direction produced by the nitrogen flow can be approximated as a transport by a constant downward velocity $V_o < 0$. This assumption, the least justified among those utilized here, is inevitable because the only alternative for providing a full account of the influence of the nitrogen flow on heat exchange is the numerical solution of the full 2D system of equations for the gas motion, which is beyond the scope of this paper.

The other two parameters are T_{cold}, the temperature of water at the lower end of wafer, and T_{hot}, the temperature at the upper end of the wafer. T_{hot} has different meanings dependening on the kind of heating applied. In the case of gas heating it denotes the nitrogen temperature at $x = x_t$, and in the case of contact heating it is the wafer temperature itself at the top end.

The following thermal analysis incorporates simplifications based on certain physical properties of the materials under consideration. First, the thermal conductivity of semiconductor material is much higher than the thermal conductivity of water and nitrogen, *i.e.*

$$\lambda_w \gg \lambda_o. \tag{11}$$

Further, the thermal diffusion time for semiconductor material D_w^2/κ_w, is much smaller than the typical time scale of the wafer motion. Therefore, the quasi-stationary approximation can be adopted and the equations describing the diffusion and convection of heat in the system and heat exchange between the wafer and outer medium can be given as

$$\frac{D_w V_w}{2}\frac{\mathrm{d}T_w}{\mathrm{d}x} = \frac{\kappa_w D_w}{2}\frac{\mathrm{d}^2 T_w}{\mathrm{d}x^2} + \frac{2\lambda_o}{\rho_w c_{pw} D_o}(T_o - T_w), \tag{12a}$$

$$\frac{D_o V_o}{2}\frac{\mathrm{d}T_o}{\mathrm{d}x} = \frac{\kappa_o D_o}{2}\frac{\mathrm{d}^2 T_w}{\mathrm{d}x^2} - \frac{2\lambda_o}{\rho_o c_{p_o} D_o}(T_o - T_w). \tag{12b}$$

In the equations, the terms on the left-hand side and first terms on the right-hand side are the usual expressions for convection and diffusion of heat in the vertical direction. The second terms on the right-hand side describe the heat exchange between the wafer and the outer medium. Taking into account (11) and applying Newton's cooling law, we approximate the conductive horizontal heat flux per unit length as the averaged horizontal temperature gradient in the gap $(T_o - T_w)/(D_o/2)$ multiplied by the thermal conductivity of the outer medium λ_o. Convective heat flux in the horizontal direction is neglected, which corresponds to the assumption of laminar, primarily vertical motion of nitrogen and water in the gap.

For the boundary conditions at the lower end $x = x_b$ we use Newton's cooling law for the wafer and a fixed temperature for the water

$$\frac{\mathrm{d}T_w}{\mathrm{d}x}(x_b) = \frac{1}{\delta}\frac{\lambda_o}{\lambda_w}(T_w(x_b) - T_o(x_b)), \quad T_o(x_b) = T_{\mathrm{cold}}. \tag{13}$$

The value of the constant δ, which has the dimensions of length and stands for the unknown thickness of temperature boundary layer, was arbitrarily set to 1 mm. It has to be noted that the actual value of this constant is of negligible importance because the ratio of the heat transfer at the wafer ends to the total heat exchange between the wafer and the outer medium described by the second terms on the right-hand sides of (12a–12b) is very small (of the same order of magnitude as the ratio wafer width / wafer height).

The boundary conditions at the upper end $x = x_t$ depend on the type of heating. For gas heating we have

$$\frac{\mathrm{d}T_w}{\mathrm{d}x}(x_t) = -\frac{1}{\delta}\frac{\lambda_o}{\lambda_w}(T_w(x_t) - T_o(x_t)), \quad T_o(x_t) = T_{\mathrm{hot}}, \tag{14}$$

whereas in the case of contact heating we require the fixed wafer temperature and zero heat flux in nitrogen to obey

$$T_w(x_t) = T_{\mathrm{hot}}, \quad \frac{\mathrm{d}T_o}{\mathrm{d}x}(x_t) = 0. \tag{15}$$

At the contact point $x = 0$ between water and nitrogen, the conditions of equal temperature and equal vertical heat flux must be satisfied, which is expressed by

$$T_{\mathrm{water}}(0) = T_{\mathrm{nitrogen}}(0), \quad \lambda_{\mathrm{water}}\frac{\mathrm{d}T_o}{\mathrm{d}x}|_{x<0} = \lambda_{\mathrm{nitrogen}}\frac{\mathrm{d}T_o}{\mathrm{d}x}|_{x>0}. \tag{16}$$

The system (12–16) allows an analytical solution, which, however, contains many coefficients arising because of the matching of four separate solutions of the convection-diffusion equation. Therefore, we employ a numerical solution. The differential equations are replaced by their finite-difference approximations on the grid of 10^4 equally-spaced points x_i and are solved by means of the matrix version of the double-sweeping (Thomas) algorithm.

In spite of the great degree of simplification, the one-dimensional thermal model is a useful tool for obtaining the data required by the other parts of the model. The vertical distribution of wafer temperature $T_w(x)$ at $x < 0$ is used as a temperature boundary condition for a water flow under the meniscus. A very important parameter is the gradient of water temperature ∇T_c at the contact point $x = 0$. This gradient is employed in (23) to evaluate the gradient τ_0 of the

surface-tension coefficient responsible for the Marangoni reduction of the rest film thickness h_0.

Another important parameter produced by the thermal analysis is the mean water temperature at the meniscus, say T_c, necessary to evaluate the water surface-tension coefficient σ_0, viscosity μ, and density ρ. The mean surface values of these properties enter the solutions for the shape of the meniscus and the entrainment region in Section 2.5 and for the water flow in Section 2.6. There is a complication connected with the fact that the surface temperature can be redistributed and, thus, T_c can be changed by the water flow. To avoid the iteration procedure required for an exact solution of such a problem, we approximate the surface temperature as $T_c = (T_o(0) + T_w(0))/2$. This approximation has been found to be reasonable in our calculations. The calculations have also shown that the actual temperature variation along the surface does not exceed 1 K.

2.5. Meniscus and entrainment regions

In this section, a method for defining the shape of the free surface of the water between the moving wafers is discussed. We apply the model, which was first introduced by Landau and Levich [5] and Bretherton [6] for the case with constant surface tension and developed later by Wilson [7] and Thess and Boos [3] to include the variable surface tension due to the surfactant or non-isothermal effects. The model was also extensively used to describe the flow in Hele-Shaw cells (see *e.g.* [8], [9]). Only cursory description is provided below. A thorough analysis can be found, for example, in [7] and [8].

Making use of the separation between the length scales h_0 and ℓ_0 we divide the surface into three regions. They are the meniscus region far from the wafer wall, the entrainment (remaining film) region as $x \to \infty$, and the transition region in between. The Stokes equations (6–7) are solved separately in each region with corresponding boundary and matching conditions.

In the entrainment region, we take the advantage of slow vertical variation ($\partial/\partial x \ll \partial/\partial y$) and assume that the velocity field has only one non-zero component $v_x(y)$. Further, we assume that the film thickness in the entrainment region is constant, *i.e.* $h = h_0$. (This assumption can be considered as a definition of the entrainment region.) The solution is trivial but incomplete since the constant h_0 is unknown. We discuss in this section how this constant, which is of primary importance for the evaluation of drying efficiency, can be determined through the solution for the free surface.

We take advantage of the small capillary number (3) and apply the method of asymptotic expansions. The variables in the meniscus and transition regions are scaled, respectively, as

$$(x, y, h) = (\ell_0 X, \ell_0 Y, \ell_0 H), \quad \boldsymbol{u} = V_w \boldsymbol{U}, \quad p = \frac{\sigma}{\ell_0} P, \tag{17}$$

and

$$\begin{aligned}(x, y, h) &= \left(\ell_0(\mathrm{Ca}^{1/3}\bar{X} + X_c), \ell_0 \mathrm{Ca}^{2/3}\bar{Y}, \ell_0 \mathrm{Ca}^{2/3}\bar{H}\right), \\ &(u_x, u_y) = (V_w \bar{U}_x, V_w \mathrm{Ca}^{1/3}\bar{U}_y), \quad p = \frac{\sigma}{\ell_0}\bar{P},\end{aligned} \tag{18}$$

where capital letters are used to denote dimensionless variables and X_c is an unknown boundary between the meniscus and transition regions.

In the leading (zero) order of approximation in Ca, the problem reduces to two ordinary differential equations. In the meniscus region, the fluid flow has no effect on the shape of the

free surface at this order of approximation. The shape is determined by a purely hydrostatic balance between the pressure and surface tension. This is expressed by the equation

$$2X + K_0 = \frac{H_{XX}}{(1 + (H_X)^2)^{3/2}}, \tag{19}$$

where K_0 is the curvature of the surface at the point $X = 0$, *i.e.* at the symmetry axis of the gap between wafers. Equation (19) is a classical result [10, p.243] modified to suit our particular geometry. Applying the boundary conditions

$$H(X) = D_0/2\ell_0 \ \text{ at } X = 0, \quad H_X(X) \to -\infty \ \text{ as} X \to 0,$$

we find the solution

$$H(X) = d - \left[\frac{X(2 - K_0X - X^2)}{K_0 + X}\right]^{1/2} + A^{1/2}\Big\{E(Q, L) - F(Q, L)\Big\}, \tag{20}$$

where F and E are the elliptic integrals of the first and second kinds, respectively, and A, Q, L are defined as

$$A = \frac{1}{2}[4 + K_0^2 + K_0(8 + K_0^2)^{1/2}],\ Q = \arcsin\left[\left(\frac{AX}{2(K_0 + X)}\right)^{1/2}\right],\ L = \frac{[K_0 - (8 + K_0^2)^{1/2}]^2}{[K_0 + (8 + K_0^2)^{1/2}]^2}.$$

The unknown constant K_0 stands for the curvature of the surface at $X = 0$, *i.e.* at the symmetry axis of the gap between wafers.

In the transition region we have

$$\frac{\bar{H}^3}{3}\bar{H}_{\bar{X}\bar{X}\bar{X}} - \frac{M}{2}(\bar{H}^2 - \bar{H}_0^2) + (\bar{H} - \bar{H}_0) = 0, \tag{21}$$

where

$$M \equiv \frac{\tau_0\ell_0}{\sigma_0 \mathrm{Ca}^{1/3}} = \frac{\tau_0}{\sigma_0^{1/6} g^{1/2}\rho^{1/2}V^{1/3}\mu^{1/3}} \tag{22}$$

gives the ratio between the Marangoni force and the viscous stress due to the moving wafer. In (22), τ_0 is the absolute dimensional value of the gradient of the surface-tension coefficient due to the inhomogeneity of surface temperature. We approximate the derivative along the surface by the x-derivative and employ the linear dependence of the surface tension coefficient on the temperature (2) to obtain

$$\tau_0 \approx -\frac{\mathrm{d}\sigma}{\mathrm{d}x} = \gamma\frac{\mathrm{d}T}{\mathrm{d}x}, \tag{23}$$

where $\mathrm{d}T/\mathrm{d}x$ stands for the derivative of water surface temperature. In the thin transition region adjacent to the wafer wall, this derivative can be approximated by the derivative of the horizontally averaged wafer temperature, $\mathrm{d}T_w/\mathrm{d}x$. The distribution $T_w(x)$ is obtained through the one-dimensional thermal analysis discussed in the previous section. It has been found that, typically for the Marangoni devices considered in this paper, the gradient $\mathrm{d}T_w/\mathrm{d}x$ changes only slightly with x in the transition region. Therefore, we make a further simplification and substitute the value of $\gamma\ \mathrm{d}T_w/\mathrm{d}x$ at the contact point x_c for the x-dependent τ_0. Accordingly, the parameter M is hereafter considered a constant.

Note that, at $M = 0$, (21) reduces to the equation derived by Landau and Levich [5] for the case without Marangoni effects.

The solution in the transition region must match the constant-thickness solution for the entrainment film as $\bar{X} \to \infty$. Corresponding conditions are

$$\bar{H} \to \bar{H}_0, \quad \bar{H}_{\bar{X}} \to 0, \quad \bar{H}_{\bar{X}\bar{X}} \to 0 \qquad \text{as } \bar{X} \to \infty. \tag{24}$$

Further, we apply the matching conditions at the boundary X_c between the meniscus and transition regions (see [7] for more details)

$$H(X_c) = 0, \qquad H_X(X_c) = 0, \qquad H_{XX}(X_c) = \bar{H}_{\bar{X}\bar{X}}(\bar{X} \to -\infty). \tag{25}$$

First, two conditions in combination with (20) allow us to define the constant K_0 to give $X_c = [(K_0^2 + 4)^{1/2} - K_0]/2$. The third condition in (25) completes the formulation of a boundary-value problem for the transition region since we can apply

$$\bar{H}_{\bar{X}\bar{X}} \to (K_0^2 + 4)^{1/2} \quad \text{as} \quad \bar{X} \to -\infty. \tag{26}$$

The solution of (21) with the boundary conditions (24), (26) is found numerically by means of the shooting method. First, we choose the starting point $\bar{X}_{\text{ini}}$ so that it provides a negligibly small second term in the asymptotic solution of Equation (21):

$$\bar{H} = \bar{H}_0 + \exp[-(3 - 3M\bar{H}_0)^{1/3}\bar{X}\bar{H}_0{}^{-1}] \quad \text{as} \quad \bar{X} \to \infty. \tag{27}$$

The calculations start with an arbitrary initial value of the film thickness $\bar{H}_0$. The Runge-Kutta marching technique is applied to solve (21). The solution is calculated in the direction of decreasing $\bar{X}$ until $\bar{H}$ becomes larger than a prescribed limit value and $\bar{H}_{\bar{X}\bar{X}}$ converges to a constant $a(\bar{H}_0)$. We apply a standard shooting procedure, repeating the numerical solution with different values of $\bar{H}_0$ to find the value corresponding to $a(\bar{H}_0) = (K_0^2 + 4)^{1/2}$.

As a result, the remaining film thickness $\bar{H}_0$ can be found as a function of the parameter M. At $M = 0$, the Landau-Levich result [5] is recovered. At $M > 0$, the thickness decreases monotonically with M, which is obviously a manifestation of the positive effect of the Marangoni force we are seeking. The properties τ_0, σ_0, ρ, and μ that determine the value of M are functions of the temperature distributions. Hence, the thermal model described in Section 2.4 provides the possibility of evaluating M and h_0 as functions of the external parameters of the system, such as T_{hot}, V_w, or V_o. One interesting result found in our simulations is that two effects are of considerable importance for the increase of the Marangoni number and, thus, for the ultimate effect of thermal Marangoni drying. The first of these is the growth of the surface-tension gradient τ_0 due to the growth of $\mathrm{d}T_w/\mathrm{d}x$. The second effect is the decrease of the viscosity μ through the growth of the temperatures $T_w(x)$ and $T_o(x)$ at the contact point $x = 0$.

2.6. Flow under meniscus

In this section, we discuss the numerical solution for the water flow and temperature distribution in the area under the meniscus. As in Section 2.5 we take an advantage of small Reynolds number and apply Equations (6–8) to describe the flow. We restrict our considerations to the area immediately under the meniscus (less than $3D_o$ below the surface) and do not take into account the complications arising when the wafer is almost completely pulled out of the water and the length of its part immersed in water is comparable with the length of the domain

under consideration. Therefore, the assumptions of stationary flow and of infinite length of wafer adopted in Section 2.5 can be retained.

It is convenient to use the stream function-vorticity formulation of the Stokes equation. The stream function Ψ is defined by

$$U_x = \frac{\partial \Psi}{\partial y} \qquad U_y = -\frac{\partial \Psi}{\partial x}$$

so that the incompressibility condition (7) is automatically satisfied. It is easy to see that

$$\Delta \Psi = -\omega, \tag{28}$$

where ω is the transverse vorticity component

$$\omega = \frac{\partial U_y}{\partial x} - \frac{\partial U_x}{\partial y}. \tag{29}$$

Applying the *curl*-operator to the Stokes equations, we obtain the equation

$$\Delta \omega = 0. \tag{30}$$

The convection-diffusion equation for the temperature field $T(x, y)$ is given by (8).

The problem is solved in the domain ABCD (see Figure 4) bounded by the meniscus surface, wafer wall, symmetry axis, and an artificial inflow-outflow boundary. The shape of the free surface CD is found in Section 2.5 by the static approximation and is given by (20). A fictitious inflow-outflow boundary AB is chosen far enough from the upper surface so that it does not affect the solution in the area adjacent to the meniscus.

Boundary conditions closing the problem are the following:

At the symmetry axis [AD] we have:

$$\Psi = 0, \qquad \omega = 0, \quad \text{and} \quad \frac{\partial T}{\partial y} = 0.$$

At the free surface [CD], the conditions

$$\Psi = 0 \quad \text{and} \quad -\mu\omega = \mu \frac{\partial U_\tau}{\partial n} = \frac{\partial \sigma}{\partial s} = -\gamma \frac{\partial T}{\partial s}$$

are valid, where n and s are the normal and tangential coordinates, and U_τ is the tangential velocity component. To impose the temperature boundary condition at the free surface we recall that the thermal conductivity of water is much higher than the thermal conductivity of nitrogen and apply Newton's cooling law

$$\lambda_{\text{water}} \frac{\partial T}{\partial n} = -\lambda_{\text{nitrogen}} (T - T_{\text{nitrogen}}) \frac{1}{\delta},$$

where T_{nitrogen} is the temperature at the surface obtained using the one-dimensional thermal analysis. The thickness of a temperature boundary layer of nitrogen above the surface is set arbitrarily to 1 mm. A more accurate value could be obtained from the solution for the flow of nitrogen, which is beyond the scope of the present paper. As a justification, we invoke the results of the one-dimensional thermal analysis which give this order of magnitude for δ estimated as a thickness of the region of strong gradient of $T_o(x)$ at $x \to 0^+$.

At the moving wafer wall [BC] we have

$$\Psi = 0.$$

Here we suppose that the outflow rate through the entrainment film is negligible. For vorticity we adopt

$$\omega = -\frac{\partial^2 \Psi}{\partial y^2} \tag{31}$$

and take into account the no-slip condition $\partial\Psi/\partial y = U_x = V_w$ when calculating the second derivative of Ψ.

Various numerical approximations of the vorticity boundary condition (31) at a rigid wall are known. We tested Tom's condition, lower relaxation method (see [11]), and the condition

$$\omega_0 = \frac{2}{(y_2 - y_0)^2 - (y_1 - y_0)^2}[V_w(y_2 - y_1) + \Psi_1 - \Psi_2], \tag{32}$$

where subscripts denote the grid points numbered with the distance to the wall. Numerical experiments have shown that (32) provides the scheme with the best stability properties in the case of our problem.

Employing the fact that the thermal conductivity of semiconductor is much higher than that of water, we reduce the temperature boundary conditions at the wafer wall to $T = T_w$ and use the results of the one-dimensional thermal analysis discussed above for the wafer temperature distribution $T_w(x)$.

The right choice of the inflow boundary conditions at [AB] is very important. For the velocity field we suppose that x-derivatives are negligible in comparison with y-derivatives. In this case one can use

$$\frac{\partial \Psi}{\partial x} = \frac{\partial \omega}{\partial x} = 0 \text{ at } [AB]. \tag{33}$$

An alternative is to prescribe the polynomial expression for Ψ (the polynomial of 3rd degree satisfying $\partial^2\Psi/\partial y^2 = 0$ and boundary conditions at A and B) and use $\omega = -\Delta\Psi$ for the vorticity. Test calculations have shown that both formulations are equally stable and converge to the same final solution.

For the temperature we assume independence of the y-coordinate and use $T = T_w$ at [AB], where T_w is the wafer temperature at the same x. As can be seen in the examples of velocity and temperature fields presented in the next section , there is an obvious contradiction between such a boundary condition and the nature of the solution itself. To check the possible influence of this boundary condition on the solution, we performed several calculations with the parameter sets differing only by the distance $|AD|$. It was found that the flow and temperature distributions in the meniscus area are virtually unaffected by the inflow boundary condition as soon as the distance $|AD|$ exceeds the gap size D_o.

The system of Poisson equations (28–30), (8), with the corresponding boundary conditions is solved by use of an iterative procedure which is facilitated considerably if we introduce a fictitious time t and reformulate the problem as that for a non-stationary flow. Each iteration can be then formulated as

$$\frac{\omega^{n+1} - \omega^n}{\Delta t} = \Delta\omega^{n+1}, \frac{T^{n+1} - T^n}{\Delta t} = \kappa\Delta T^{n+1} - V^n \nabla T^n, \Delta\Psi^{n+1} = -\omega^{n+1}.$$

The time step Δt is of importance for stability properties only and is taken between 0·001 and 0·01 in the calculations.

To solve the Equations (34) we apply the method of conforming structured spectral elements [12] that combines the geometrical flexibility of finite-element methods with exponential convergence of a spectral approximation. A detailed description of the method can be found, for example, in [13].

The solution domain was discretized by a grid of 4×4 spectral elements with 5×5 test functions in each element (see Figure 4). That gives a total of 400 nodal points. The size of elements adjacent to the wafer wall and to the free surface was decreased considerably in comparison with the other elements in order to ensure concentration of the grid points in the regions of largest velocity and temperature gradients.

Certain numerical problems arise because the solution (20) for the shape of free surface has a singular peak at the point given as point C in Figure 4. In principle, the vorticity must be infinite at this point. Numerically, this leads to an instability when ω becomes too large in the vicinity. There are different ways to treat this problem. The simplest one that is also suitable for our problem is to change the geometry slightly and correct the form of the free surface $x = f(y)$ (f is a reciprocal function to $h(x)$ used in Section 2.5) at point C (corresponding to $y = y_0$), making the peak not so "sharp". Two procedures are used.

Correction 1: $f'(y_0)$ is set to $f'(y_1)$ and $f(y_0)$ to the linear interpolation

$$f(y_1) + (f(y_1) - f(y_2))\frac{(y_0 - y_1)}{(y_1 - y_2)}[V_w(y_2 - y_1) + \Psi_1 - \Psi_2], \tag{34}$$

Correction 2: $f'(y_0)$ is set to zero. Accordingly, $f(y_0) = f(y_1)$.

We have found that these corrections only affect the velocity field in the flow region in the immediate vicinity of C and, therefore, are of negligible importance for the temperature distribution. Moreover, the difference between the velocity fields obtained with different correction procedures is very small. Correction 2 is preferable because it provides faster convergence of the solution.

3. Sample calculations

Extensive calculations were performed to study the influence of different operating parameters on the efficiency of thermal Marangoni drying. In this paper we present two sample calculations, which demonstrate the ability of our model to capture the essential processes of heat and mass transfer in the system.

Both examples deal with the technique that employs gas heating. It has to be noted that, even though contact heating has proved to be, in general, more efficient, the gas-heating method remains preferable from a technological point of view. The reason is that gas-heating competely eliminates the problem of possible damage to the wafer due to contact.

The following hypothetical values of parameters were chosen in both these calculations (see Figures 1 and 3 for notation): $T_{\text{cold}} = 295$ K, $T_{\text{hot}} = 345$ K, $D_w = 1$ mm, $D_o = 3$ mm, $V_w = 1$ mm s^{-1}, $x_t - x_b = 200$ mm. The different parameters were the position of wafer relative to the water surface as defined by the coordinates x_t and x_b and the horizontally averaged vertical velocity of nitrogen V_o. Our simulations have shown that the influence of

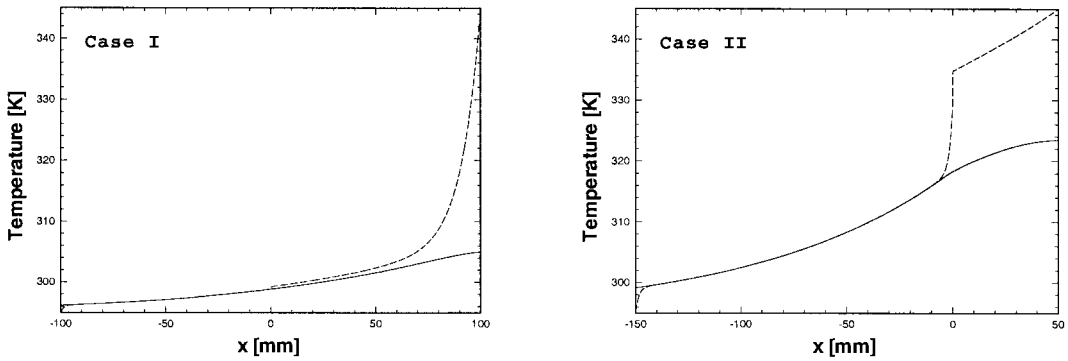

Figure 5. Sample results of the one-dimensional thermal analysis. Horizontally averaged temperature of wafer (solid curves) and outer medium (water at $x < 0$ and nitrogen at $x > 0$, shown as dashed curves) as functions of the vertical coordinate x.

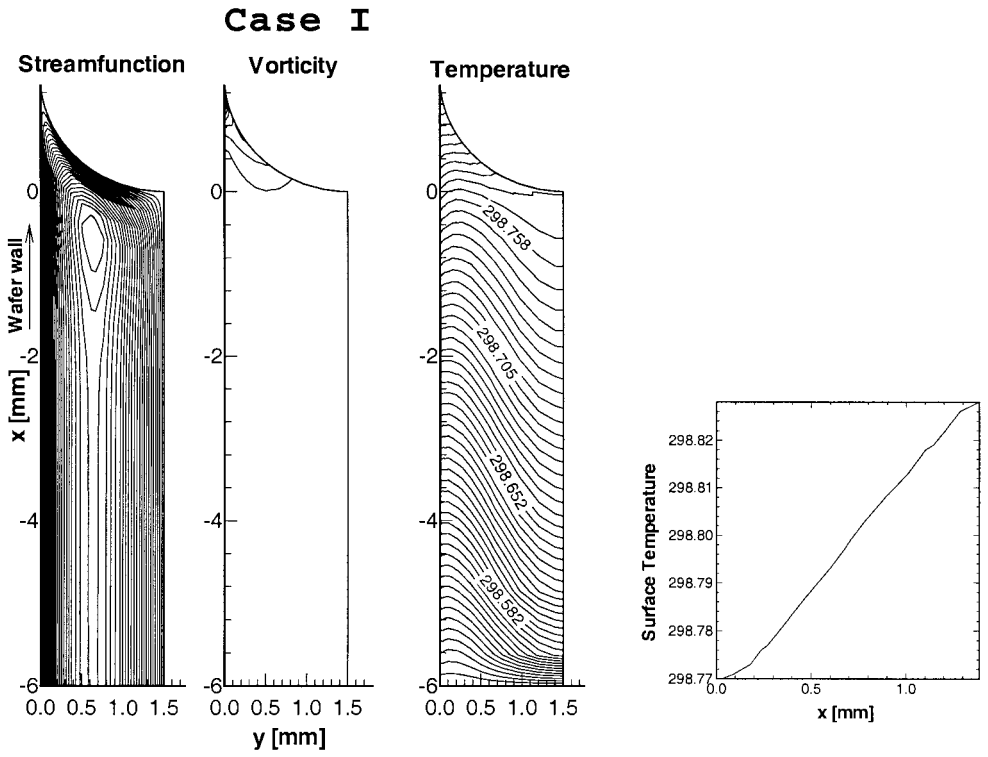

Figure 6. Isolines of streamfunction Ψ, vorticity ω, and temperature T, and plot of surface temperature *vs.* vertical coordinate x are shown for the Case I. For the isolines, positive levels are plotted as solid lines, negative levels - as dashed lines. For stream function, positive (negative) values correspond to clockwise (counter-clockwise) circulation.

x_t and x_b, except when they take their extreme values, is rather weak. On the other hand, the nitrogen velocity V_o has been found to have the largest impact on the efficiency of drying. V_o defines the intensity of pumping the nitrogen into the gap between wafers, which is decisive for heating the upper part of the wafer and, thus, for creating a strong temperature gradient on the water surface.

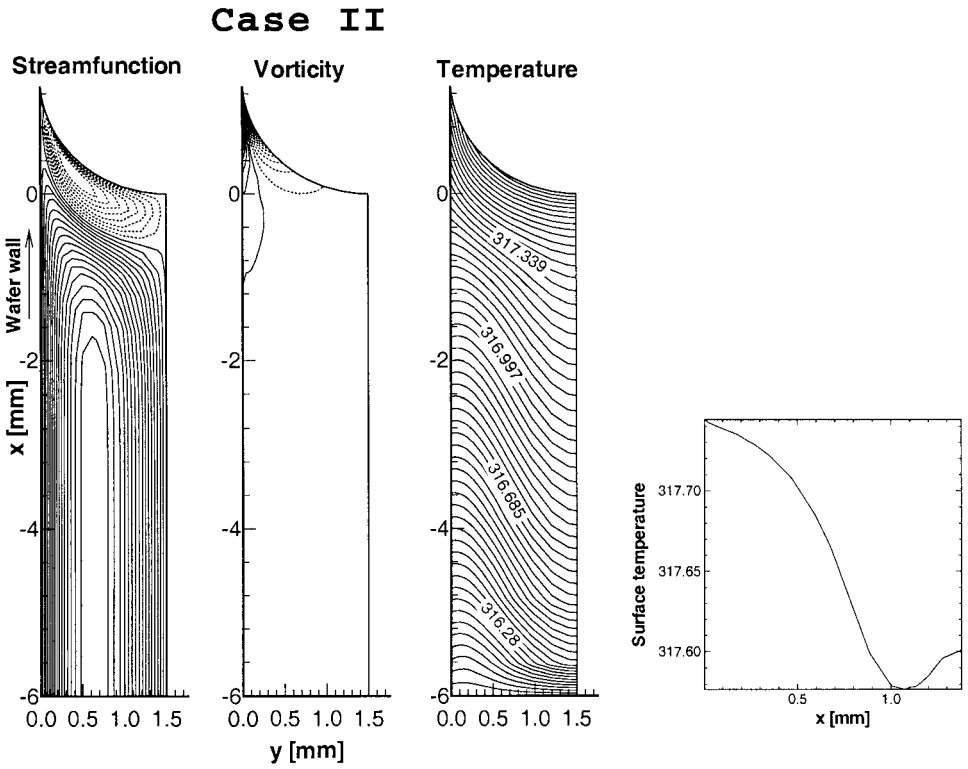

Figure 7. Sample results of calculations of water flow under the meniscus. Solution for the Case II is plotted as in Figure 6.

Hereafter we consider Case I corresponding to $x_b = -100$ mm, $x_t = 100$ mm and $V_o = -100$ mm s^{-1} and Case II with $x_b = -150$ mm, $x_t = 50$ mm and $V_o = -1000$ mm s^{-1}. The results of the one-dimensional thermal analysis, i.e., the solutions to Equations (12a), (12b) with respective boundary conditions are shown in Figure 5. The shape of the temperature curves is determined to a large degree by the fact that the thermal condutivities of nitrogen, water, and semiconductor material differ by orders of magnitude,

$$\lambda_{\text{nitrogen}} \ll \lambda_{\text{water}} \ll \lambda_{\text{wafer}}.$$

The wafer acts as a kind of heat exchanger furnishing the effective heat transfer in the vertical direction. The intensities of the horizontal heat fluxes, from nitrogen to wafer at $x > 0$ and from wafer to water at $x < 0$ are defined, apart from the temperature differences, by the values of $\lambda_{\text{nitrogen}}$ and λ_{water}. One can see in Figure 5 that λ_{water} is high enough to allow an almost perfect heat equilibrium between the wafer and water layers. On the other hand, the layer of nitrogen, which has a thermal conductivity about twenty times lower than that of water, is not able to produce an energy influx to the wafer competitive with the vertical heat flux in the wafer itself and the convective heat transfer by the nitrogen vertical velocity V_o. As a result, there is an essential difference between the mean temperatures of wafer and nitrogen.

Using the wafer temperature at the contact point $T_c(0)$ and its vertical gradient $\nabla T_c(0)$ as input parameters, we can apply the analysis of Section 2.5 and find the shape of the meniscus and the solution for the entrainment and transition regions. After calculating the asymptotic thickness h_0 of the remaining film, we evaluate the efficiency of thermal Marangoni drying

as the ratio of h_0 to the thickness obtained in the system kept at a constant temperature 295 K (0·95 μm for the configuration considered here). For Case I and Case II this ratio is, respectively, 0·98 and 0·66. Two remarks concerning this reduction of h_0 are in order. First, only a part of the reduction owes its existence to the action of the Marangoni force. The other, non-negligible part is due to the fact that the water viscosity decreases considerably (down to 50%) with the increasing temperature at the surface. Second, we do not take into account the evaporation at the surface of the remaining film, which can be quite intensive at temperatures like those shown in Figure 5 for Case II.

Figures 6 and 7 show the velocity and temperature fields calculated for Cases I and II by means of the numerical procedure of Section 2.6. Apart from a peculiarity discussed below, the flow patterns are quite reasonable. The flow in the meniscus area created by the joint action of the Marangoni force and wafer movement consists primarily of the circulation in the clockwise direction. The cold fluid is driven upwards along the wall of the wafer, heated due to contact with the wafer and the hot nitrogen, and flows downwards along the symmetry axis. The strongest vorticity is concentrated around the contact point between the wafer and the meniscus.

A striking feature of the velocity field shown in Figure 7 is the large circulation zone near the meniscus surface (note that the main circulation still reaches the surface as a thin stripe near the wafer wall). Such recirculation is typical for cases when hot nitrogen is pumped deeply into the gap between wafers. The reason is that the temperature of nitrogen at the meniscus surface is very high, much higher than that of the wafer cooled by the water (*cf.* Figure 5, Case II). This results in a considerable heat flux into the water, which creates a surface temperature profile growing with the distance to wafer and, thus, a Marangoni force directed from the symmetry axis to the wafer. Even if this force is rather weak, it can reverse the very slow flow caused by the wafer motion. This flow development is undesirable, because the particles to be removed from the wafer wall are not carried away effectively. Some of them stay close to the wall.

4. Concluding remarks

In this paper we have formulated and tested a theoretical model for the technological process of thermal Marangoni drying applied in the processing of semiconductor materials. The model has proved to be able to capture the main mechanisms acting in the system and produce estimates useful for engineering applications. Comparison with experimental results, details of which are proprietary information and can not be given here, shows good agreement.

An important feature of our work is that we do not try to study the different physical processes separately. Instead, we integrate the diversified physical models using a set of input-output parameters and consider the whole system starting with the operating parameters and concluding with estimates for the efficiency of drying and the velocity and temperature fields.

The questions of technical feasibility of thermal Marangoni drying and of the impact of different parameters on the efficiency are not addressed in the present paper. The examples considered in Section 3 allow the conclusion that the thermal Marangoni effect does indeed work. We can therefore hope that a drying device based upon this effect may be feasible with an optimum choice of operating parameters.

References

1. J. Marra and J.A.M. Huethorst, Physical Principles of Marangoni Drying *Langmuir* 7 (1991) 2748–2755.
2. K. Wolke, B. Eitel, M. Schenkl, S. Ruemmelin, and R. Schild, Marangoni wafer drying avoids disadtvantages. *Solid State Technology* 8 (1996) 87–90.
3. A. Thess and W. Boos, A model for Marangoni drying. *Phys. Fluids* 11 (1999) 3852–3855.
4. K. Wolke and M. Weber, *Verfahren und Vorrichtung zum Trocknen von Substraten*. Patent No. DE19800584 A, Germany, (17 July 1999).
5. L.D. Landau and V.G. Levich, Dragging of a liquid by a moving plate. *Acta Physico-Chim. USSR* 17 (1942) 42–45.
6. F.P. Bretherton, The motion of long bubbles in tubes. *J. Fluid Mech.* 10 (1961) 166–188.
7. S.K. Wilson, The effect of an axial temperature gradient on the steady motion of a large droplet in a tube. *J. Eng. Math.* 29 (1995) 205–217.
8. C.-W. Park and G.M. Homsy, Two-phase displacement in Hele Shaw cells: theory. *J. Fluid Mech.* 139 (1984) 291–308.
9. C.V. Park, Effects of insoluble surfactants on dip coating. *J. Colloid Interf. Sci.* 146 (1991) 382–394.
10. L.D. Landau and E.M. Lifshitz, *Fluid Mechanics*. Pergamon Press (1987) 537pp.
11. C.A.J. Fletcher, *Computational Techniques for Fluid Dynamics.* Springer-Verlag (1991) 493 pp.
12. O. Zikanov, Spectral-element code for flow simulations *Internal Report of Inst. for Aerospace Eng., TU Dresden* (1998).
13. K.Z. Korczak and A.T. Patera, An isoparametric spectral element method for solution of the Navier-Stokes equation in complex geometry. *J. Comp. Phys.* 62 (1986) 361–381.